20 V Stack of Aqueous Supercapacitors with Carbon (−), Titanium Bipolar Plates and CNT-Polypyrrole Composite (+)

Xiaohang Zhou, Chuang Peng, and George Z. Chen
Dept. of Chemical and Environmental Engineering, and Energy and Sustainability Research Div., Faculty of Engineering, University of Nottingham, Nottingham, NG7 2RD, U.K.

DOI 10.1002/aic.12632
Published online June 20, 2011 in Wiley Online Library (wileyonlinelibrary.com).

A 20 V stack of 19 supercapacitors was fabricated from titanium bipolar plates (150 × 150 × 0.1 mm^3) coated on each side with carbon nanotubes and polypyrrole composite (+) and pigment carbon black (−), and microporous polymeric separators containing aqueous KCl. Internal sealing of each cell in the stack was achieved by placing a silicone rubber washer between neighboring bipolar plates. The stack was tested by high voltage cyclic voltammetry, galvanostatic charging and discharging, and electrochemical impedance spectroscopy. It approached 25 kW/kg in maximum specific power and 3.64 Wh/kg in specific energy. Performance of the stack through intermittent charging-discharging tests in a storage period of 10 months (still ongoing) remained fairly stable. For example, it exhibited almost zero decay in capacitance after 1000 continuous galvanostatic charging-discharging cycles in the first month of storage (10 V), and less than 6% loss in the seventh month (19 V). © 2011 American Institute of Chemical Engineers *AIChE J,* 58: 974–983, 2012
Keywords: aqueous supercapacitor stack, titanium bipolar plates, carbon nanotube, polypyrrole, carbon black

Introduction

As new energy storage devices, supercapacitors (or electrochemical capacitors) are generally perceived to be capable of attaining higher energy densities than conventional capacitors and higher power densities than batteries.[1–5] Their applications are commonly designed for systems that can benefit from fast charging and discharging, and from pulsed power boosting, such as camera flash and electric automotive acceleration.

Like all electrochemical energy conversion and storage devices, including batteries and fuel cells, supercapacitors usually have a single cell voltage ranging typically from 1.0 to 3.5 V. Such limits result mainly from either the over-oxidation or -reduction of the active materials on the electrodes, or the decomposition of a component of the electrolyte, particularly the solvent. The electrolytes used in supercapacitors can be either aqueous or organic. Aqueous electrolytes offer advantages in terms of affordability, higher conductivity, large heat capacity, and low environmental impact, but they often have lower working voltages (1.0–2.0 V) than those organic ones (2.0–4.0 V). To achieve high voltages as required by many power devices, an effective and simple approach is to serially stack the cells through bipolar electrodes. This approach is commonplace in fuel cells,[6–8] but it was applied only in a few cases of symmetrical supercapacitors with a solid electrolyte.[9,10] The effort was recently extended to stacks of asymmetrical supercapacitors with an aqueous electrolyte.[11] It is worth pointing out that in these previous studies, the dimensions of the actually fabricated stacks were

Correspondence concerning this article should be addressed to G. Z. Chen at george.chen@nottingham.ac.uk.

relatively small with the stack voltage being less than 10 V. The active materials used were either activated carbon or transition metal oxides. Although silicone rubber[10] or epoxy resin[11] was used to externally seal the stack, little was reported about the charging-discharging cyclability and storage stability of the supercapacitor stacks.

This article presents the design, fabrication, and experimental tests of stacked aqueous asymmetrical supercapacitors at a significantly large scale than those in previous studies.[9,10] With micro-porous polymeric separators containing an aqueous electrolyte, sealing of the stack was achieved internally in each cell by a silicon rubber washer between two neighboring bipolar plates. To avoid corrosion attacks by the aqueous electrolyte, thin titanium foils were used as the bipolar plates. As the core materials in this research, a commercial pigment carbon black, and a laboratory-made nanocomposite of conducting polymer and carbon nanotubes (CNTs) were attached to the negative and positive electrodes, respectively, by the solution cast and evaporation method.

Carbon-based materials of high specific areas possess large double layer capacitance and also exploitable pseudo-capacitance if appropriately functionalized.[2,3,12,13] They are especially attractive from an economic point of view. In aqueous electrolytes, hydrogen evolution on carbon requires in general a fairly high overpotential.[11] Thus, to extend the working voltage of aqueous asymmetrical supercapacitors, carbons are often used to make the negative electrode in conjunction with, for example, a conducting polymer based positive electrode.[14–17]

The most commonly used conducting polymers include polyaniline (PANi), polypyrrole (PPy), and poly[3,4-ethylenedioxythiophene] (PEDOT).[3] Upon doping, they have good electrical conductivity and large pseudo-capacitance arising from the fast and reversible redox processes related to the π conjugated polymer chains.[3,18] The specific capacitances and potential ranges for capacitive performance were reported to be 775 F/g and 0.65 V for PANi,[3,19] 480 F/g and 1.0 V for PPy,[3,20] and 210 F/g and 1.0 V for PEDOT.[3,21,22] Thus, of these three polymers, PPy would offer the highest energy capacity. When used as the positive electrode, these polymers lose electrons during charging (oxidation), causing the anions in solution to intercalate into the electrode to maintain electro-neutrality. Depletion of the anions occurs when the process is reversed during discharging (reduction). However, ion intercalation and depletion in the polymer can lead to strain variation at microscopic levels, which can accumulate into fatigue degradation of the polymer after repeated charge-discharge cycles. This is a particular drawback of conducting polymers in which the conjugated π bonds contribute to the rigidity of the polymer chains. Consequently, conducting polymers are mechanically far less flexible than their σ-bond based nonconducting counterparts and structurally unable to withstand repeated microscopic strain variations. Because ion movements into and from the conducting polymer are inevitable during charging and discharging, the cycle life of supercapacitors can be compromised.

An effective measure against the low mechanical strength and stability of conducting polymers is to combine it with CNTs.[1–4,23] Unlike the conducting polymer itself, the composite remains electronically conductive in the undoped state of the conducting polymer because electrons can flow through the interconnected CNTs. For ion conduction in the composite, it would be ideal if all the individual CNTs are coated by a thin layer (<100 nm) of the polymer and connected into a three dimensional network. In such a composite, the micro- and nano-pores between the coated CNTs provide efficient pathways for fast ion movements in the electrolyte contained in the pores. Also, the thin polymer coating on the CNT means a short time for ion intercalation and depletion. These structural features were indeed recently confirmed to be beneficial to improving the storage capacity and charge-discharge rates.[24,25] It should be pointed out that, like conducting polymers, CNTs are also rich in conjugated π bonds and can be anionized through partial oxidation, i.e., formation of surface hydroxyl and carboxylic groups by acid treatment and deprotonation of these groups at appropriate pH levels. Thus, they can interact very well with the conducting polymer which is cationic in the doped state, introducing additional benefits to the efficiency of the synthesis process and the charge storage capacity in the produced nanocomposites.[26,27]

The use of titanium bipolar plates is the other important aspect of this work. Being the fourth most abundant metallic element in the earth's crust, titanium is as strong as steel but 45% lighter, whist twice stronger than aluminium and only 60% heavier.[28] It has high resistance to corrosion, particularly in aqueous solutions containing chloride ions which can attack both stainless steels and aluminium. Titanium is also sufficiently ductile for fabrication into thin plates. These properties are ideal for applications of the metal as the electrode substrate or bipolar plate in electrochemical energy storage devices.[29,30] The main concern is the cost of using titanium. In the current market, titanium (ca., \$15,000/tonne) is far more expensive than stainless steel (ca., \$3,900/tonne on average) and aluminium (ca., \$2,600/tonne).[31–33] Nevertheless, research for alternative and cheaper routes for titanium production has continued ever since early 1950s when commercial production of titanium started through the metallothermic reduction or the Kroll process.[34,35] Particularly, in the past decade, there are a number of innovative approaches for extraction of titanium directly from its oxide (TiO_2) in molten salts, promising favorable commercial competition with aluminium and stainless steels.[36] This prospect of emerging technologies for economical production and the desirable properties of titanium formed the basis for using titanium bipolar plates in the aqueous asymmetrical supercapacitors of this work.

Experimental

Acid treatment of carbon nanotubes

Multi-walled CNTs, 10–30 nm in diameter and 5–15 μm in length, were purchased from Shenzhen Nanotech Port Co., Ltd, and acid treated according to literature.[2,3,37] Briefly, the as-received CNTs were boiled in concentrated sulphuric and nitric acids (3:1 v/v) for 20 min to introduce surface functional groups, and to remove metallic impurities (catalysts) and amorphous carbon. The produced mixture was cooled, washed with deionized water in a filter crucible (grade 4.5) until the pH reached 7, and dried overnight at

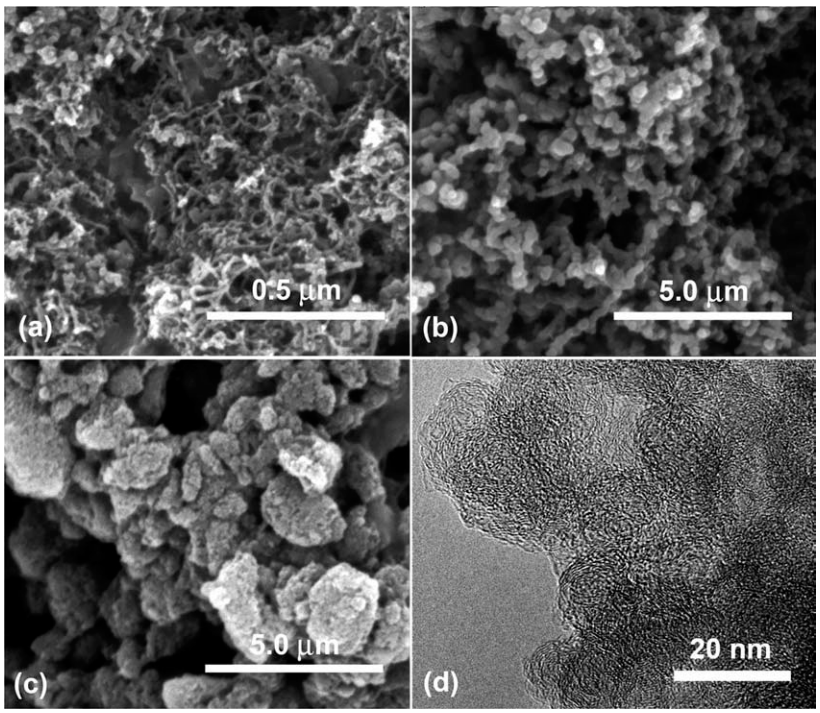

Figure 1. SEM images of (a, b) the PPy-CNT nanocomposites synthesized in 500 mL (a) and 100 mL (b) deionized water, and (c) the CMPB. (d) TEM image of the CMPB.

50°C in an oven. Such treated CNTs could be ground to a fine powder with mortar and pestle, and re-dispersed in water readily.

Active electrode materials

The composite of PPy and CNTs was used as the positive electrode material in this work. It was synthesized as follows. The acid treated CNTs (0.5 g) were dispersed in deionized water (500 mL), yielding a suspension containing 0.1 wt % CNTs. Pyrrole (2 g, Aldrich) was added into the suspension, followed by sonication for 20 min. Another solution was prepared by dissolving 10 g anhydrous ferric chloride ($FeCl_3$, Sigma) in 50 mL deionized water. The $FeCl_3$ solution was added, under stirring, into the pyrrole-CNT suspension drop by drop at an interval of 1 s. The mixture was then filtered. The black filtrand was washed until the water became colorless, dried at 40°C for 24 h, weighed, and finally ground to a fine powder.

Scanning electron microscopy (SEM, FEI-QUANTA 600, FEI) revealed that the PPy coated CNTs had an average diameter of 130 nm and 374 nm if synthesized in 500 mL and 100 mL of deionized water as shown in Figures 1a, b, respectively. This finding suggests a simple way of controlling the thickness of the PPy coating on individual CNTs. Because of the larger particle sizes as shown in Figure 1b, the PPy-CNT composite made in 100 mL water could not disperse in water to form a stable suspension, and hence will not be further discussed in this article. All results reported below are obtained from that synthesized in 500 mL water.

The Cabot Monarch 1300 pigment black (CMPB), which is a specialty activated carbon used as a pigment in black inks or paints, was used as received to prepare the negative electrode. Dispersion of the CMPB in water or an aqueous electrolyte could be readily achieved by ultrasonication. SEM and high resolution transmission electron microscopy (HRTEM, JEOL JEM-2100F) images revealed that, the CMPB contained loosely packed micro-sized agglomerates (Figure 1c), of which each was composed of uniform onion-like carbon nanoparticles (8–12 nm) (Figure 1d).

Electrochemical characterizations of the active electrode materials

A graphite rod (purity $>$ 99%; diameter $=$ 6.0 mm) was covered by epoxy resin, leaving the two ends open. After polishing, one of the open ends was used as a disc working electrode (0.283 cm^2). The same graphite rod without the epoxy coating was used as the counter electrode, and an Ag/AgCl (3 mol/L KCl) electrode as the reference.

The PPy-CNT nanocomposite (100 mg) synthesized in 500 mL water was thoroughly mixed with 5 wt % polyvinyl alcohol (PVA) and then dispersed in deionized water (2 mL). It is worth mentioning that PVA was used in this work as a hydrophilic binder to assist wetting of the active material by the aqueous electrolyte. This mixture (20 μL) was then dropped on the graphite disc working electrode and dried in air to form a thin coating equivalent to 3.53 mg/cm^2. The PPy-CNT modified electrode was characterized in the conventional three-electrode cell by cyclic voltammetry (CV), galvanostatic charging and discharging (GCD), and electrochemical impedance spectroscopy (EIS) (Autolab PGSTAT30, EcoChemie, Netherlands) in the aqueous solution of 3.0 mol/L KCl at room temperature. The EIS was conducted in the frequency range of 0.01 to 10,000 Hz at a designated bias potential. The CMPB was studied in the

same way and exhibited similar electrochemical properties as other activated carbons as reported in the literature.

Construction and characterizations of stacked asymmetrical supercapacitors

A 20 V stack was constructed from 19 "PPy-CNT (+) | 3.0 mol/L KCl | CMPB (−)" cells connected in series through titanium bipolar plates (150 mm × 150 mm × 0.1 mm). In this laboratory, the specific capacitance of the CMPB was found to be in the range of 80–100 F/g. For the PPy-CNT nanocomposite, the variation of the specific capacitance was similar, from 130 to 160 F/g. In both cases, the actual value of the specific capacitance depended on the methods of electrochemical measurement.

In designing the asymmetrical supercapacitor, the lower specific capacitance values of the CMPB (80 F/g) and the PPy-CNT composite (130 F/g) were used so that the actual performance of the supercapacitor would not be inferior to the design. Thus, if the capacitances of the positive and negative electrodes need to be comparable, the following equation applies,

$$C_+ \times M_+ = C_- \times M_- \quad (1)$$

where C_+ and C_- are the specific capacitances, and M_+ and M_- the masses of the PPy-CNT nanocomposite and the CMPB on the positive and negative electrodes, respectively.

According to Eq. 1, 0.27 g PPy-CNT nanocomposites with 5 wt % PVA were thoroughly dispersed in 5 mL deionized water and painted over an area of 120 mm × 120 mm on one side of the titanium bipolar plate. After drying in air for a few hours, this mixture of PPy-CNT and PVA formed a stable and fairly uniform coating, equivalent to 1.88 mg/cm^2, on the surface of the titanium plate, which was to function as the positive electrode, see Figure 2a. Then, 0.44 g pigment black with 5 wt % PVA were dispersed in 5 mL deionized water and painted over an area of 120 mm × 120 mm on the opposite side of the titanium bipolar plate as the negative electrode. The mass loadings on both positive and negative electrodes should give a single cell capacitance of 17.6 F. After drying, the bipolar plate loaded with the positive and negative active materials was assembled into the stack as described below.

Following the same procedure, 18 titanium bipolar plates loaded with the active materials on each side were prepared. The end plates of the stack were prepared similarly as the bipolar plates, but only one side was painted with the pigment black (negative) or the PPy-CNT composite (positive). These 18 bipolar and 2 end plates were assembled layer by layer into a stack of 19 cells. It was always the positive side of one plate facing the negative side of a neighbor. A porous separator (130 mm × 130 mm filter paper, Whatman grade 1) which was presoaked in the aqueous solution of 3 mol/L KCl was placed between each pair of neighboring plates. A silicone rubber washer was cut from a thin sheet (0.3 mm in thickness) with a window of 130 mm × 130 mm, and a width of 10 mm on each side to surround the four sides of each separator for sealing against water evaporation. The stacked cells were held together by 16 pairs of screws (50 mm) and wingnuts between two stainless steel supporting plates (180 mm × 180 mm × 5 mm), see Figure 2b. Electric

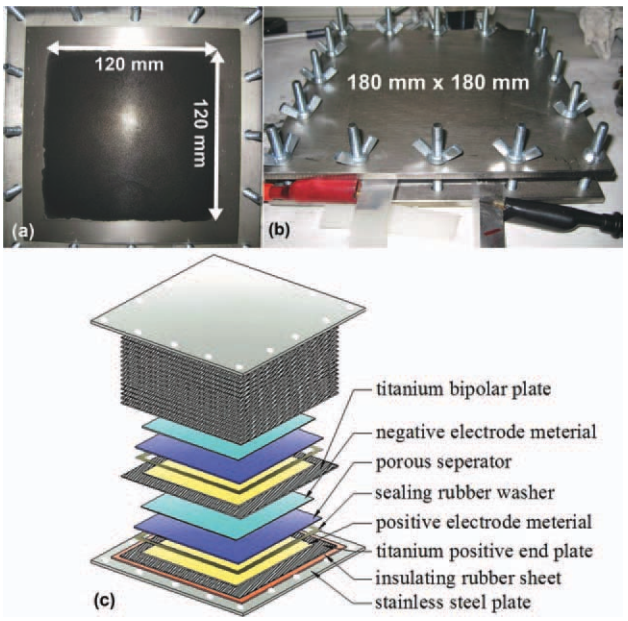

Figure 2. Photographs of (a) a middle titanium bipolar plate in the stack loaded with the active material (PPy-CNT composite), and (b) the stack of 19 "PPy-CNT (+) | 3 mol/L KCl | CMPB (–)" supercapacitors connected through titanium bipolar plates. (c) The expanded schematic illustration of the bipolarly connected stack.

The stainless steel supporting plates and the titanium bipolar plates of the stack were 180 mm × 180 mm × 5 mm and 150 mm × 150 mm × 0.1 mm in dimensions, respectively. The areas covered by the active material were 120 mm × 120 mm. [Color figure can be viewed in the online issue, which is available at wileyonlinelibrary.com].

insulation between the stainless steel and titanium plates was achieved by a thick silicon rubber sheet (150 mm × 150 mm × 3 mm). Figure 2c illustrates schematically the stack with each of the components. Upon completion of assembly, the thickness of the stack, including all components, could be adjusted between 23 and 25 mm through manually losing or tightening the wingnuts, which means that the thickness of each cell in the stack would be about or less than 0.5 mm. The stack thickness is thus indicative of the relative pressure in the stack. In this work, the stack thickness was maintained at 24.5 mm in most experiments but slightly decreased to check the effect of increasing pressure on the performance of the stack.

The stack was characterized in principle by CV, GCD, and EIS. A voltage multiplier (Metrohm Autolab B.V., Netherlands) was used to extend the voltage range of the potentiostat to over 20 V. In addition, self-discharge was studied by firstly charging the stack at a designated voltage for 10 min, and then monitoring the open circuit voltage (OCV) decay with time.

Results and Discussion

Capacitive behavior of the PPy-CNT nanocomposite

The PPy-CNT nanocomposite was reported previously to exhibit good capacitive behavior in aqueous electrolytes.[2,3]

This finding was re-confirmed by CV, GCD and EIS (Nyquist plot[38,39]) in this work as shown in Figure 3. Nevertheless, the CV reveals that the current switching at the positive potential end is faster than that at the negative potential end, in agreement with the PPy in the composite being less conductive in the reduced state at negative potentials. Similarly, the GCD also shows the *i*R drop in the charging process, but not in discharging. Clearly, if the PPy-CNT composite is used as the positive electrode in a supercapacitor, it is necessary to avoid discharging the electrode to very negative potentials. More discussion on this point will be given later in this article.

From Figure 3, the electrode capacitance can be derived by the following equations for each of the technique used.

$$C_{CV} = mC_S = \frac{Q}{2U} \tag{2}$$

$$C_{GCD} = mC_S = \frac{i}{dE/dt} \tag{3}$$

$$C_{EIS} = mC_S = \frac{1}{2\pi f(-Z'')} \tag{4}$$

where Q is the total charge enclosed in the CV, U the potential window, dE/dt the average slopes of the charging (increasing potential) and discharging (decreasing potential) curves, i the applied constant current; f the frequency, Z'' the imaginary impedance, and m the mass of the PPy-CNT nanocomposite on the electrode. The specific capacitance as derived from these three methods were comparable to each other, ranging between 130 and 160 F/g, largely depending on the rate of charging-discharging.

Performance of bipolarly stacked "PPy-CNT (+) | 3 mol/L KCl | CMPB(–)" supercapacitors

Cyclic Voltammograms. Figure 4a shows the CV plots of the stack of 19 "PPy-CNT (+) | 3 mol/L KCl | CMPB(–) aqueous supercapacitors with titanium bipolar plates. It can be seen that at all applied scan rates (200, 600, and 1000 mV/s), the CV plots are all highly rectangular in shape between 0.0 and 20.0 V, indicating the inherent characteristics of a supercapacitor and also fast electrode kinetics and low internal resistance. In comparison with Figure 3a, the more ideal capacitive behavior demonstrated in Figure 4a might have resulted from two factors. First, the CV plots in Figure 4a reflect the combined contribution of the PPy-CNT positive electrodes, and the CMPB negative electrodes. Activated carbons, such as the CMPB, are capable of behaving in an ideal capacitive manner and hence can contribute to mitigation of the nonideal capacitive behavior of PPy-CNT. Second, the potential in Figure 3a extends to −0.5 V (vs. Ag/AgCl), which must have invoked significant PPy reduction, and hence nonideal capacitive behavior as evidenced by Figure 3a. However, in Figure 4a, even at the discharging end of the voltage window, i.e., 0 V, the potential of the PPy-CNT electrodes was unlikely more negative than −0.1 V. This is because at equal capacitance, the CMPB negative and PPy-CNT positive electrodes would share equally the voltage in each cell. Because the stack was charged to 20 V at maximum, the voltage shared by each cell would be 1.05 V. Thus, the PPy-CNT electrodes would be at 0.5 V (vs. Ag/AgCl) in the charged state, and –0.025 V at the discharged state. (Similarly, the CMPB electrodes would be at –0.5 V in the charged state and 0.025 V at the discharged state.) As a consequence, the PPy-CNT electrodes in the stack were never reduced as much as in the three electrode cell for recording Figure 3a, and hence remained highly conducting and capacitive.

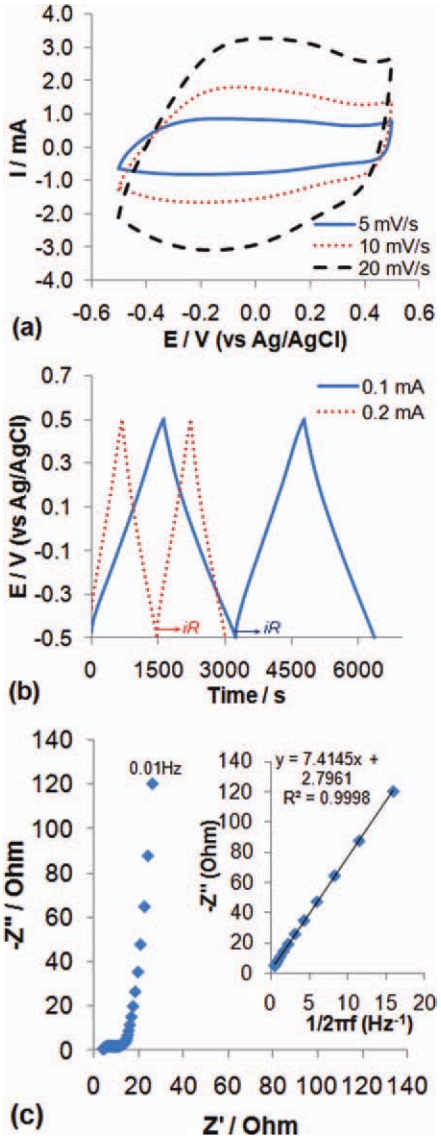

Figure 3. Electrochemical characterizations of the PPy-CNT nanocomposite (1 mg on 6 mm graphite disc electrode) in 3 mol/L KCl. (a) CV plots at scan rates as indicated. (b) GCD plots at constant currents as indicated. (c) Nyquist plot at 0 V (vs. Ag/AgCl) between 10 mHz and 10 kHz.

The inset in (c) plots the imaginary impedance against the reciprocal of the frequency. [Color figure can be viewed in the online issue, which is available at wileyonlinelibrary.com].

It is worth mentioning that because the stack contained 19 cells, the applied voltage scan was theoretically shared equally by each cell, e.g., 1000 mV/s for the stack but 53

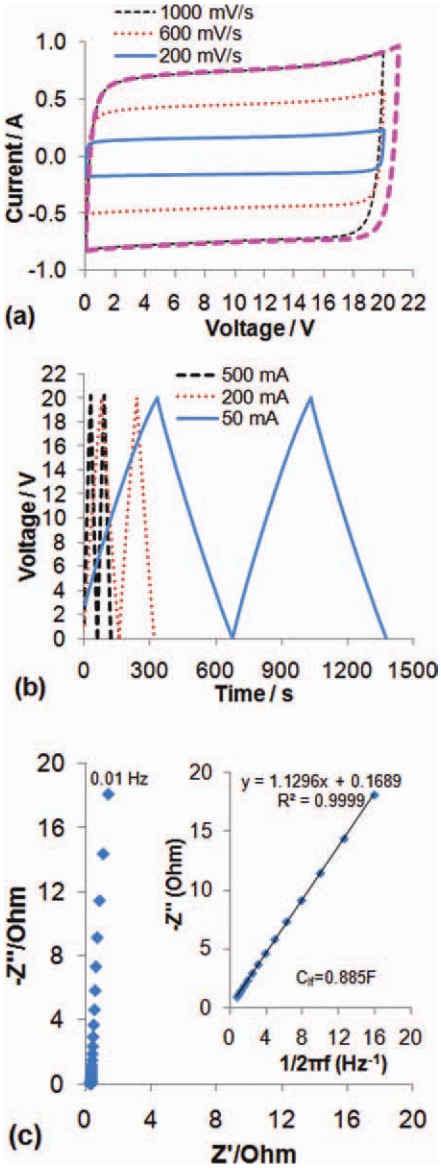

Figure 4. Electrochemical characterizations of the stack of 19 "PPy-CNT (+) | 3 mol/L KCl | CMPB (–)" supercapacitors connected through titanium bipolar plates. (a) CV plots at scan rates as indicated. (b) GCD plots recorded at currents as indicated. (c) Nyquist plot at 0 V between 10 mHz and 10 kHz.

The inset in (c) plots the imaginary impedance against the reciprocal of the frequency. [Color figure can be viewed in the online issue, which is available at wileyonlinelibrary.com].

mV/s for each cell. This stack feature is an advantage over a single cell in practice when fast voltage change and large voltage range are needed. The CV plots in Figure 4a can also be used to derive the capacitance of the stack according to Eq. 2 and the results are listed in Table 1. The stack capacitance increased slightly with decreasing the scan rate and may be attributed to the same cause as explained before.

Table 1. Capacitances Derived from CV Plots of the Stack of 19 "PPy-CNT (+) | 3 mol/L KCl | CMPB (–)" Aqueous Supercapacitors Connected by Titanium Bipolar Plates (cf. Figure 4a)

Scan rate (mV/s)	200	600	1000
Capacitance (F)	0.792	0.750	0.731

Galvanostatic Charge-discharge. Figure 4b shows the results from GCD measurements of the stack between 0 and 20 V with very linear voltage-time relationships at the three currents applied. On these plots, the stack voltages at time = 0 varied and did not start at 0 V possibly due to the same cause as explained before. In the second charging-discharging cycle, however, no sign of *i*R drop was observed, suggesting very small equivalent series resistance (ESR).

The capacitance of the stack can also be derived from the GCD plots according to Eq. 3. Table 2 lists the results, showing that the capacitance of this stack increases slightly with decreasing the applied current, reflecting again the effect of ionic movement in the electrodes. The coulombic efficiencies at all the currents applied were very high, increasing from 96.4% at 50 mA to 99.7% at 500 mA. Because the capacitance was higher at a lower current, the increased coulombic efficiency may be due to the electrode reaction involving less internal active material on the electrode, and hence becoming more reversible.

Assuming equal capacitive contribution from each electrode in the stack as designed, the capacitance of the stack can be calculated by Eq. 5 as follow.

$$C_{\text{stack}} = \frac{C_{\text{single}}}{n} \tag{5}$$

where C_{stack} is the capacitance of stack, C_{single} the capacitance of each individual eletrode, and n the number of cells. Thus, at 50 mA, each cell could have a capacitance of 16.8 F, and the specific capacitances would be 124 F/g for PPy-CNT and 76 F/g for CMPB. Considering experimental errors, particularly manual fabrication and operation, the designed and experimentally measured single cell capacitances, and the specific capacitances of PPy-CNT and CMPB in the 19 cell stack agree very well with each other, which signifies a success in scaling up and bipolarly stacking the PPy-CNT | 3 mol/L KCl | CMPB aqueous supercapacitors.

Electrochemical Impedance Spectroscopy. The stack was further studied by EIS and Figure 4c presents the typical result. The plot is dominated by the tilted straight line at low

Table 2. Charges Derived from the Second GCD Cycles of the Stack of 19 Aqueous Supercapacitors of PPy-CNT (+) | 3 mol/L KCl | CMPB (–) Connected by Titanium Bipolar Plates, and the Respective Coulombic Efficiencies and Capacitances (cf. Figure 4b)

Current (mA)	Apparent Current Density (mA/cm^2)	Charge (C)	Discharge (C)	Coulombic Efficiency (%)	Average Capacitance (F)
50	0.35	17.92	17.27	96.4	0.88
200	1.39	16.21	15.90	98.1	0.80
500	3.47	15.35	15.30	99.7	0.77

frequencies from which C_{EIS} was derived to be 0.885 F according to Eq. 4. It is also noticed that Figure 4c exhibits the absence of any charge transfer barrier (semicircle) at high frequencies. Again, as in the case of GCD plots, this observation can be explained as follows. In the discharged state of the stack, the PPy-CNT electrodes were not as deeply reduced as that in the experiment for recording Figure 3c, and hence remained highly conducting and exerting little kinetic influence on charge transfer. This understanding could also explain the very small intercept, 0.30 Ω, of the Nyquist plot at the horizontal axis as shown in Figure 4c.

Maximum Specific Power and Specific Energy. The aforementioned high frequency resistance is effectively the ESR of the stack and can be used to calculate the maximum specific power, P_{max}, according to Eq. 6 below,[11]

$$P_{max} = \frac{U^2}{4mESR} \tag{6}$$

where U and C are the stack voltage and capacitance, and m the total mass of the active materials on both positive and negative electrodes (= 13.49 g). At 20 V, $P_{max} = 24.71$ kW/kg.

The specific energy, E_S, of the stack can be derived from its capacitance, C, and the working voltage, U, of the stack from the following equation,

$$E_S = \frac{CU^2}{2m} \tag{7}$$

As discussed above, the stack capacitance varied slightly between 0.885 F (EIS at 0 V) and 0.880 F (GCD at 50 mA) according to the CV, GCD and EIS measurements. Thus, with $U = 20$ V and $m = 13.49$ g, it can be calculated from Eq. 7 that the value of E_S is greater than 3.64 Wh/kg.

Self-discharge. Like all electrochemical energy storage devices, supercapacitors are known to undergo self-discharge in storage under open circuit conditions.[40,41] Self-discharge is thermodynamically spontaneous, although its occurrence is decided by kinetics and mechanisms.[40] In this work, self-discharge was studied by firstly charging the 19 cell stack at a designated voltage for 10 min, and then monitoring the OCV decay with time. Figure 5a presents the OCV-time plots after charging the stack at 19 V (circles) and 10 V (squares), respectively, for 10 min. For comparison, the OCV-time plot of a commercial 2.5 V and 5 F supercapacitor (Jinzhou Fu-Chen Supercapacitor Co. Ltd, China) is presented in Figure 5b, recorded after charging at 2.5 V for 10 min.

In Figure 5a, for charging at 19 V, the OCV of the stack exhibits a fast drop to ca., 14 V in the first hour, followed by a slow decay to ca., 10 V over a long period (up to 7.5 h). This behavior is very similar to that of the commercial supercapacitor in Figure 5b, suggesting similar mechanisms. In Figure 5a, the two plots demonstrate clearly that self-discharge becomes slower at lower stack voltages. This feature is more evident on the OCV-time plot of the stack charged at 10 V (squares) which shows the OCV decay was obviously slower.

Self-discharge can follow different mechanisms and are strongly case dependent, although three main causes have been identified: (1) localized reactions on electrodes due to the presence of redox active impurities (e.g., dissolved oxygen gas and transition metal ions), (2) diffusion controlled cycles of electro-active impurities between positive and negative electrodes, and (3) current leakage through internal and/or external "short circuits". These mechanisms can each present unique OCV-time features according to Eqs. 8–10 below,[40]

$$V_{OC} = a - b\ln(t + c) \qquad \text{(localized redox reaction)} \tag{8}$$

$$V_{OC} = V^o_{OC} - A\sqrt{t} \qquad \text{(diffusion controlled redox cycling)} \tag{9}$$

$$V_{OC} = V^o_{OC}\exp\left(\frac{-t}{R_L C}\right) \qquad \text{(current leakage)} \tag{10}$$

where V_{OC} and t are the OCV and time, respectively, and the others are all constants with specific physical meanings for a given system.[40] Particularly, the current leakage mechanism represented by Eq. 10 was claimed to occur more likely to bipolar plates connected cells with improper sealing.[40] To identify the causes for the self-discharge of the 19 cell stack, in comparison with that of the commercial product, the OCV-time plots were fitted by each of Eqs. 8–10. It was found that only the fittings by Eq. 8 produced satisfactory results as superimposed in Figures 5a, b. This finding suggests strongly localized redox reactions to be responsible for the self-discharge of both the 19 cell stack and the single cell commercial cell. It also implies that there was insignificant current leakage in the 19 cell stack.

Effect of Pressure. In this work, changing pressure in the stack was achieved by adjusting the 16 holding screws. Figure 5c compares the CV plots of the stack recorded before (low pressure) and after (normal pressure) the screws were fully tightened manually. In response, the stack's thickness decreased by about 3 mm before and after tightening. In comparison with the CV plot under the normal pressure, the CV plot under a low pressure was noticeably less rectangular with the current switching at both positive and negative potential ends being significantly slower, indicative of a greater internal resistance. The capacitance also became smaller slightly by decreasing the pressure, from 0.820 F to 0.769 F. These changes in response to the pressure variation could be explained by the improved contact between the active materials and the titanium bipolar plates. Also, because each cell was sealed in the stack, increasing the pressure could help force the electrolyte into previously unoccupied pores in the active materials. Of course, the improved performance as shown in Figure 5c calls for more quantitative experimental and analytical approaches.

Charging-discharging Cycle Stability. In continuous potential cycling of the stack, as shown in Figure 6a and 6**b**, no change was observed between the 2nd and 1000th CV plots in the 0 V to 10 V range. The decay in current was also fairly small amongst the 2nd, 10th, and 1000th CV plots in the 0 V to 19 V range. The relative capacitance changes against that of the 2nd CV are plotted against the number of voltage cycles in Figure 6c. It can be seen that the capacitance remained highly constant in the 10 V range, and decreased by only 6% after 800 cycles and then became steady in the following cycles in the 19 V range. It is worth mentioning that the results in Figure 6 were recorded at a

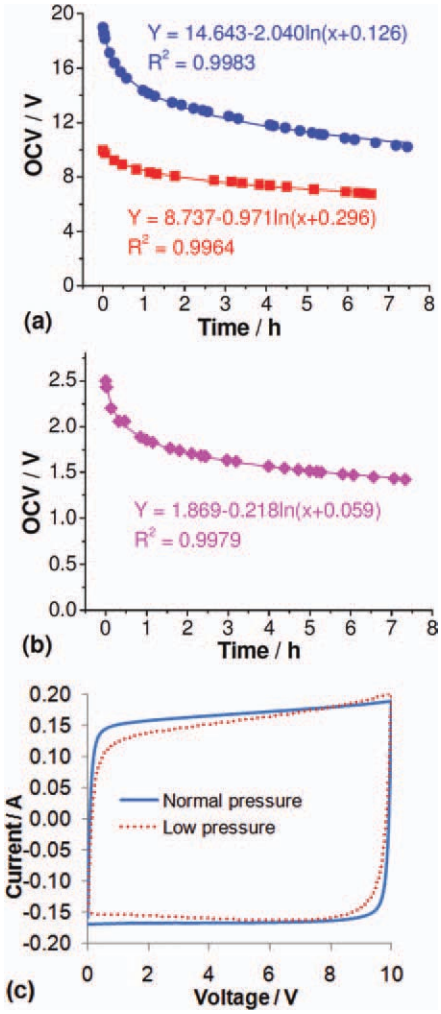

Figure 5. (a) The OCV-time plots of the stack of 19 "PPy-CNT (+) | 3 mol/L KCl | CMPB (–)" supercapacitors connected through titanium bipolar plates, after charging at 19 V (circles) and 10 V (squares) for 10 min. (b) The OCV-time plot of a commercial supercapacitor (2.5 V, 5 F), after charging at 2.5 V for 10 min. In both (a) and (b) are superimposed the nonlinear fitting results according to Eq. 8.[40] for the localized redox reaction mechanism. (c) CV plots of the stack at a scan rate of 200 mV/s under "normal" and "low" pressures achieved by manually adjusting the holding screws of the stack.

[Color figure can be viewed in the online issue, which is available at wileyonlinelibrary.com].

voltage scan rate of 200 mV/s on the stack, or ca., 10.53 mV/s per cell, which is fairly slow. Thus, the completion of 1000 cycles took more than 26 h, during which performance decay may also result from water evaporation as discussed in the next section. In agreement with this explanation, it was found that after the 1000 cycles of charging-discharging and overnight or longer storage in the desiccator, some of the lost capacitance shown in Figure 6c could be recovered. For example, the stack capacitance at the end of the 1000 cycle between 0 and 19 V in Figure 6c was 0.77 F, but after storage in the desiccator, the capacitance recovered back to beyond 0.80 F.

Storage Stability. The performance of the 19 cell stack has been monitored intermittently in a storage period of 13 months during which various tests have been conducted (equivalent approximately to 5000 charge-discharge cycles, and these tests are still ongoing). Figures 7a–c compare, respectively, the CV, GCD, and Nyquist plots of the stack recorded in the 1st and 10th months. Whilst maintaining almost ideal capacitive features, minor differences seen between the results obtained in the 1st and 10th months include a small decrease in capacitance (which is less than 7% as can be derived from Figure 7b). Particularly, the ESR did not change significantly during the 10-month storage, as shown in Figure 7c.

An important and simple measure applied in this work for storage is that, when not in test, the 19 cell stack was always stored in a desiccator as schematically illustrated in the inset of Figure 7c. All desiccants were removed from the desiccator and a small amount of water was added to the bottom below the perforated mesh. It was observed that if stored in air for a few days, the stack would show small decay which however could be recovered after storage in the closed desiccator. Thus, water evaporation was not completely avoided by the silicone rubber washers. While manual fabrication could be a cause which can be replaced by properly designed manufacturing in commercial application, complete sealing of the stack in a seamless metal case like that used for sealing lithium ion batteries may be necessary. Another point worth mentioning is that it is known that chloride solutions can attack stainless steels and other metals, but their effect on titanium is minimized. Indeed, light rust was observed to form on the steel screws and support plates. Thus, the excellent performance of the stack recorded after 10-month storage must have been at least partly a result of the use of titanium bipolar plates.

Conclusions

This article has reported findings from designing, stacking, and testing 19 "PPy-CNT (+) | 3 mol/L KCl | CMPB (−)" supercapacitors connected in series through titanium bipolar plates. The morphology and electrochemical properties of the PPy-CNT nanocomposite were examined by SEM, TEM, CV, GCD, and EIS. The operation voltage of the 19 cell stack achieved 20 V without noticeable unwanted electrode reactions. Due to the use of an aqueous electrolyte, titanium bipolar plates, thin layers of the activated materials, sealed and tightened configuration, the ESR of this 19 cell stack could be as low as 0.30 Ω. The maximum specific power and the specific energy of the stack reached 24.71 kW/kg and 3.64 Wh/kg, respectively. The 20 V stack showed very high charging-discharging cycle stability, with the capacitance loss being almost zero in the 10 V range and less than 6% (partially recoverable) in the 19 V range after 1000 cycles. The storage stability of the stack has been tested for 10 months, again showing only a capacitance loss of less than 7%. Self-discharge was observed with the OCV

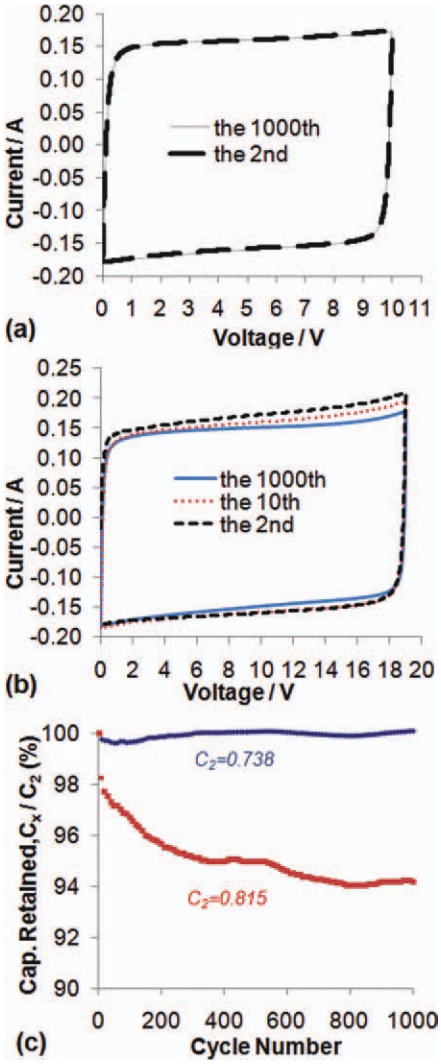

Figure 6. (a) The 2nd and 1000th CV plots of the stack of 19 "PPy-CNT (+) | 3 mol/L KCl | CMPB (–)" supercapacitors connected through titanium bipolar plates in the 1st month. (b) The 2nd, 10th, and 1000th CV plots of the stack in the 10th month. (c) Percentage of capacitance retained as calculated from the CV plots at different cycles.

1st month: C_2= 0.783 F; C_{1000} = 0.784 F. 10th month: C_2= 0.815 F, C_{1000} = 0.775 F. Scan rate: 200 mV/s. Aqueous electrolyte: 3.0 mol/L KCl. [Color figure can be viewed in the online issue, which is available at wileyonlinelibrary.com].

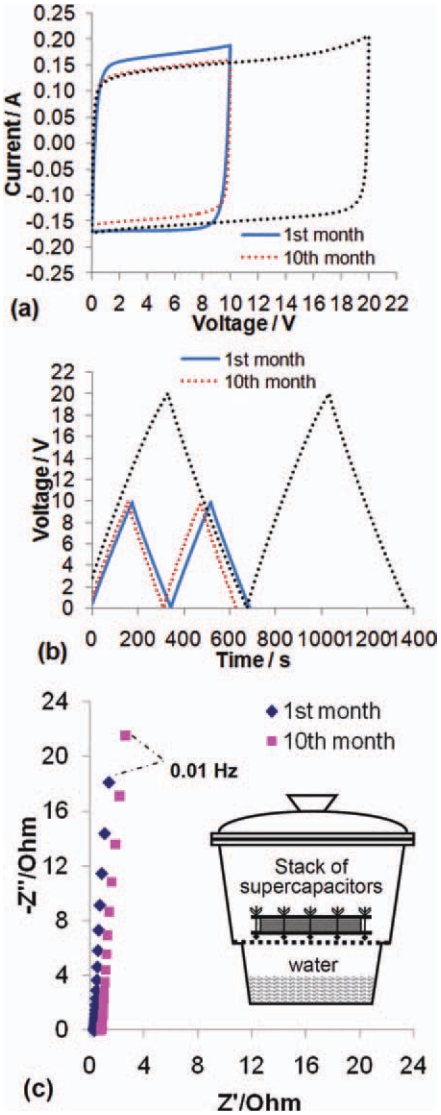

Figure 7. Electro-characterizations of the stack of 19 "PPy-CNT (+) | 3 mol/L KCl | CMPB (–)" supercapacitors connected through titanium bipolar plates in the 1st (solid lines in (a) and (b), or diamonds in (c)), and 10th months of storage and intermittent tests (dotted lines in (a) and (b), or squares in (c)). (a) CV plots at 200 mV/s. (b) GCD plots at 50 mA. (c) Nyquist plots at 0 V between 10 mHz and 10 kHz.

The inset in (c) illustrates the storage of the 19 cell stack above water in a closed desiccator. [Color figure can be viewed in the online issue, which is available at wileyonlinelibrary.com].

decreasing from 19 V to 10 V in 7.5 h, and follows the same mechanism as that in a commercial single cell supercapacitor. Nonlinear curve fitting of the OCV data revealed the self-discharge to be likely related with redox active impurities (e.g., dissolved oxygen and transition metal ions) reacting with the charged electrode materials.

A crucial contribution to these successes came from the use of titanium bipolar plates which can effectively resist the severe corrosion attack of the aqueous KCl electrolyte which, however, offered high ionic conductivity and heat capacity. Other materials used in the fabrication of the stack have all contributed to the success of this work, including filter paper as the separators and also electrolyte holder, silicone rubber as the sealing washers and electric insulators, stainless steel as the supporting plates and screws for holding the stack and adjusting pressure. It is expected that the design and testing results reported here could form the basis for future commercial applications.

Acknowledgments

The authors thank E.ON AG for funding through the E.ON International Research Initiative—Energy Storage 2007. Responsibility for the content of this article lies with the authors.

Literature Cited

1. Frackowiak E, Béguin F. Carbon materials for the electrochemical storage of energy in capacitors. *Carbon*. 2001;39:937–950.
2. Hughes M, Chen GZ, Shaffer MSP, Fray DJ, Windle AH. Electrochemical capacitance of a nanoporous composite of carbon nanotubes and polypyrrole. *Chem Mater*. 2002;14:1610–1613.
3. Peng C, Jin J, Chen GZ. A comparative study on electrochemical co-deposition and capacitance of composite films of conducting polymers and carbon nanotubes. *Electrochim Acta*. 2007;53:525–537.
4. Peng C, Zhang S, Jewell D, Chen GZ. Carbon nanotube and conducting polymer composites for supercapacitors. *Prog Nat Sci*. 2008;18:777–788.
5. Conway BE. *Electrochemical Supercapacitors: Scientific Fundamentals and Technological Applications*. New York: Kluwer Academic/Plenum Publishers, 1999.
6. Hu M, Sui S, Zhu X, Yu Q, Cao G, Hong X, Tu H. A 10kW class PEM fuel cell stack based on the catalyst-coated membrane (CCM) method. *Int J Hydrogen Energy*. 2006;31:1010–1018.
7. Rajalakshmi N, Pandiyan S, Dhathathreyan KS. Design and development of modular fuel cell stacks for various applications. *Int J Hydrogen Energy*. 2008;33:449–454.
8. Lin C, Huang L, Chiang L, Chyou Y. Thermal stress analysis of planar solid oxide fuel cell stacks: effects of sealing design. *J Power Sources*. 2009;192:515–524.
9. Lian KK, Li C, Jung RH, Kincs JG. Electrochemical cell having symmetric inorganic electrodes. *U.S. Patent* 5587872, 1996.
10. Staiti P, Lufrano F. Design, Fabrication, and evaluation of a 1.5 F and 5 V prototype of solid-state electrochemical supercapacitor. *J Electrochem Soc*. 2005;152:A617–A621.
11. Ng KC, Zhang S, Peng C, Chen GZ. Individual and bipolarly stacked asymmetrical aqueous supercapacitors of CNTs/SnO_2 and CNTs/MnO_2 nanocomposites. *J Electrochem Soc*. 2009;156:A846–A853.
12. Andreas HA, Conway BE. Examination of the double-layer capacitance of an high specific-area C-cloth electrode as titrated from acidic to alkaline pHs. *Electrochim Acta*. 2007;51:6510–6520.
13. Li H, Xi HA, Zhu S, Wen Z, Wang R. Preparation, structural characterization, and electrochemical properties of chemically modified mesoporous carbon. *Microporous Mesoporous Mat*. 2006;96:357–362.
14. Laforgue A, Simon P, Fauvarque JF, Mastragostino M, Soavi F, Sarrau JF, Lailler P, Conte M, Rossi E, Saguatti S. Activated carbon/conducting polymer hybrid supercapacitors. *J Electrochem Soc*. 2003;150:A645–A651.
15. Zhang Y, Feng H, Wu X, Wang L, Zhang A, Xia T, Dong H, Li X, Zhang L. Progress of electrochemical capacitor electrode materials: a review. *Int J Hydrogen Energy*. 2009;34:4889–4899.
16. Hu D, Peng C, Chen GZ. Electro-deposition of non-conducting polymers: Roles of carbon nanotubes in the process and products. *ACS Nano*. 2010;4:4274–4282.
17. Peng C, Zhang S, Zhou X, Chen GZ. Unequalisation of electrode capacitances for enhanced energy capacity in asymmetrical supercapacitors. *Energy Environ Sci*. 2010;3:1499–1502.
18. Gurunathan K, Murugan AV, Marimuthu R, Mulik UP, Amalnerkar DP. Electrochemically synthesised conducting polymeric materials for applications towards technology in electronics, optoelectronics and energy storage devices. *Mater Chem Phys*. 1999;61:173–191.
19. Gupta V, Miura N. High performance electrochemical supercapacitor from electrochemically synthesized nanostructured polyaniline. *Mater Lett*. 2006;60:1466–1469.
20. Fan L, Maier J. High-performance polypyrrole electrode materials for redox supercapacitors. *Electrochem Commun*. 2006;8:937–940.
21. Xu Y, Wang J, Sun W, Wang S. Capacitance properties of poly(3,4-ethylenedioxythiophene)/polypyrrole composites. *J Power Sources*. 2006;159:370–373.
22. Peng C, Zhou X, Chen GZ, Moggia F, Fages F, Brisset H, Roncali J. Internally referenced analysis of charge-transfer reactions in a new ferrocenyl bithiophenic conducting polymer through cyclic voltammetry. *Chem Commun*. 2008;6606–6608.
23. Zhang X, Zhang J, Liu Z. Conducting polymer/carbon nanotube composite films made by in situ electropolymerisation using an ionic surfactant as the supporting electrolyte. *Carbon*. 2005;43:2186–2191.
24. Frackowiak E, Jurewicz K, Szostak K, Delpeux S, Béguin F. Nanotubular materials as electrodes for supercapacitors. *Fuel Process Tech*. 2002;77–78:213–219.
25. Frackowiak E, Khomenko V, Jurewicz K, Lota K, Béguin F. Supercapacitors based on conducting polymers/nanotubes composites. *J Power Sources*. 2006;153:413–418.
26. Santhosh P, Manesh KM, Lee K, Gopalan AI. Enhanced electrocatalysis for the reduction of hydrogen peroxide at new multiwall carbon nanotube grafted polydiphenylamine modified electrode. *Electroanalysis*. 2006;18:894–903.
27. Chen GZ, Shaffer MSP, Coleby D, Dixon G D, Zhou W, Fray DJ, Windle AH. Carbon nanotube and polypyrrole composites: coating and doping. *Adv Mater*. 2000;12:522–526.
28. The A to Z of Materials. Available at: http://www.azom.com/Details.asp?ArticleID=5107. Updated July 14, 2010. Accessed May, 2010.
29. Jayakumar K, Pandiyan S, Rajalakshmi N, Dhathathreyan KS. Cost-benefit analysis of commercial bipolar plates for PEMFC's. *J Power Sources*. 2006;161:454–459.
30. Middelman E, Kout W, Vogelaar B, Lenssen J, Waal ED. Bipolar plates for PEM fuel cells. *J Power Sources*. 2003;118:44–46.
31. Isaac ED. Titaniumin in the First Quarter 2010. U.S.Geological Survey: Reston, VA, 2010.
32. Neely PR. Aluminumin April 2010. U.S. Geological Survey, Reston, VA, 2010.
33. MEPS World Stainless Steel Prices. Available at: http://www.meps.co.uk/Stainless%20Prices.htm. Updated April, 2010. Accessed May, 2010.
34. Ikeshima T. *Titanium Science and Technology*. In Lutjering G, Zwicker U, Bunk, W, editors. *Proc. 5th Int. Conf. Titanium, München 1984*, DGM-Deutsche Gesellschaft für Materialkunde e.V., 1985.
35. Kroll W. The production of ductile titanium. *J Electrochem Soc*. 1940;78:35–47.
36. Chen GZ, Fray DJ, Farthing TW. Direct electrochemical reduction of titanium dioxide to titanium in molten calcium chloride. *Nature*. 2000;407:361–364.
37. Shaffer MSP, Fan X, Windle AH. Dispersion and packing of carbon nanotubes. *Carbon*. 1998;36:1603–1612.
38. Orazem ME, Tribollet B. *Electrochemical Impedance Spectroscopy*. New Jersey: Wiley, 2008.
39. Barsoukov E, Macdonald JR. *Impedance Spectroscopy Theory, Experiment, and Applications*, 2nd ed. New Jersey: Wiley, 2005.
40. Niu J, Conway BE, Pell WG. Comparative studies of self-discharge by potential decay and float-current measurements at C double-layer capacitor and battery electrodes. *J Power Sources*. 2004;135:332–343.
41. Ricketts BW, Ton-That C. Self-discharge of carbon-based supercapacitors with organic electrolytes. *J Power Sources*. 2000;89:64–69.

Manuscript received Aug. 10, 2010, revision received Nov. 18, 2010, and final revision received Mar. 17, 2011.